optica

Optomechanical sensing of liquids outside standard fibers using forward stimulated Brillouin scattering

YAIR ANTMAN, ALEX CLAIN, YOSEF LONDON, AND AVI ZADOK*

Faculty of Engineering and Institute for Nanotechnology and Advanced Materials, Bar-Ilan University, Ramat-Gan 5290002, Israel
**Corresponding author: Avinoam.Zadok@biu.ac.il*

Received 8 February 2016; revised 8 April 2016; accepted 11 April 2016 (Doc. ID 259156); published 12 May 2016

The analysis of chemical species is one of the most fundamental and long-standing challenges in fiber-optic sensors research. Existing sensor architectures require a spatial overlap between light and the substance being tested and rely either on structural modifications of standard fibers or on specialty photonic crystal fibers. In this work, we report an optomechanical fiber sensor that addresses liquids outside the cladding of standard, 8/125 μm single-mode fibers with no structural intervention. Measurements are based on forward stimulated Brillouin scattering by radial, guided acoustic modes of the fiber structure. The acoustic modes are stimulated by an optical pump pulse and probed by an optical signal wave, both confined to the core. The acoustic vibrations induce a nonreciprocal phase delay to the signal wave, which is monitored in a Sagnac interferometer loop configuration. The measured resonance frequencies and excitation strengths of individual modes agree with the predictions of a corresponding quantitative analysis. The acoustic reflectivity at the outer cladding boundary and the acoustic impedance of the surrounding medium are extracted from cavity lifetime measurements of multiple modes. The acoustic impedances of deionized water and ethanol are measured with better than 1% accuracy. The measurements successfully distinguish between aqueous solutions with 0, 4%, 8%, and 12% concentrations of dissolved salt. The new fiber-sensing paradigm might be used in the monitoring of industrial processes involving ionic solutions.

OCIS codes: (060.2370) Fiber optics sensors; (120.4880) Optomechanics; (290.5900) Scattering, stimulated Brillouin.

http://dx.doi.org/10.1364/OPTICA.3.000510

1. INTRODUCTION

Optical fibers constitute an excellent sensing platform [1–4]. Fibers allow remote access and can be embedded within a structure under test with little effect on functionality. Fibers are also immune to electro-magnetic interference and are suitable for hazardous environments where electricity cannot be used. One of the most fundamental and widely investigated challenges in fiber sensor research is the analysis of the surrounding media [4]. The vast majority of sensing protocols monitor either the refractive index or the absorption spectrum of a substance under test. Such measurements face an inherent difficulty: the analysis mandates some degree of spatial overlap between an optical wave and the medium being studied, whereas light in standard fibers is confined to the core and does not reach the outside of the cladding.

To go around this difficulty, the fiber-optic sensors of liquids developed to date either rely on hollow-core, photonic crystal fibers (PCFs) [5–8] or involve considerable structural modifications of standard fibers. Specific forms of the latter include long-period fiber Bragg gratings for the excitation of cladding modes [9], etching or polishing fibers down to the core [10,11], tapering fibers down to few-microns diameters [12], the application of transducer coating layers [13], the fabrication of inline cavities [14], and the use of cleaved facets [15,16]. Many of these devices and setups are extremely sensitive. However, the structural interventions involved in their realization remain a major drawback. Another promising approach is the use of specialty materials, such as chemically sensitive fibers made of biopolymers or biocompatible hydrogels [17,18], silk [19], and even spider silk [20].

In this work, we propose and demonstrate, for the first time to our knowledge, the analysis of liquid media outside the cladding of a standard, 8/125 μm single-mode fiber, with no structural modifications or external transducer elements. The measurement principle is based on optomechanics: the stimulation and probing of guided acoustic modes of the fiber structure at hundreds of megahertz frequencies [21–27] by optical waves that are confined to the core. The temporal decay profile of the stimulated acoustic waves is affected by partial reflection and transmission at the outer boundary of the fiber cladding. Therefore, the acoustic impedance of the surrounding medium may be obtained based on acoustic cavity lifetime measurements. Sound waves generated by stimulated Brillouin scattering processes were previously used to penetrate the media outside of photonic devices [28–31].

In our experiments, we measure the acoustic impedances of deionized water and ethanol. The results agree with values reported in the literature to within less than 1% [32]. Further, the analysis successfully distinguishes between solutions of NaCl dissolved in deionized water, prepared with different salt weight

ratios of 0, 4%, 8%, and 12%. The dependence of the acoustic impedance on the level of salinity is in general agreement with the literature as well [33]. These last results illustrate the sensitivity of the analysis protocol and also its potential application in the monitoring of heavy ionic solutions in industrial processes. The platform represents a conceptual breakthrough in fiber-optic sensing of liquids.

2. PRINCIPLES OF OPERATION

A. Optical Stimulation and Probing of Guided Acoustic Waves in Standard Fibers

1. Radial Acoustic Modes in Standard Fibers

Standard optical fibers support several groups of guided acoustic modes [21,22]. One category is that of radial modes, denoted as $R_{0,m}$, in which the acoustic field is radially symmetric. Let us denote the radius of the fiber cladding as $a = 62.5$ μm and the acoustic velocities of the longitudinal and shear waves in silica as $V_d = 5996$ m/s and $V_s = 3740$ m/s, respectively. The cut-off frequency of mode $R_{0,m}$ is given by $f_{0,m} = [V_d/(2\pi a)]\xi_m$, where ξ_m is the mth solution to the equation [21]

$$(1 - \alpha^2)J_0(\xi) = \alpha^2 J_2(\xi), \tag{1}$$

and $\alpha \equiv V_s/V_d = 0.62$. The acoustic modes are formulated in a cylindrical coordinate system, where r is the radial coordinate and z denotes the axial position. The transverse profile of density fluctuations in mode $R_{0,m}$ is proportional to [27]

$$\Delta\rho_{0,m}(r) = J_0(\xi_m r/a). \tag{2}$$

2. Optomechanical Stimulation of Radial Acoustic Modes

Figure 1(a) shows a schematic illustration of the dispersion relation between the acoustic frequencies of modes $R_{0,m}$ and their axial wavenumbers $q_{z,m}$ [25]. Immediately above the cutoff, the modes are entirely transverse, and their group velocity component in the z direction approaches zero. In contrast, the axial phase velocity can become arbitrarily large close to $f_{0,m}$.

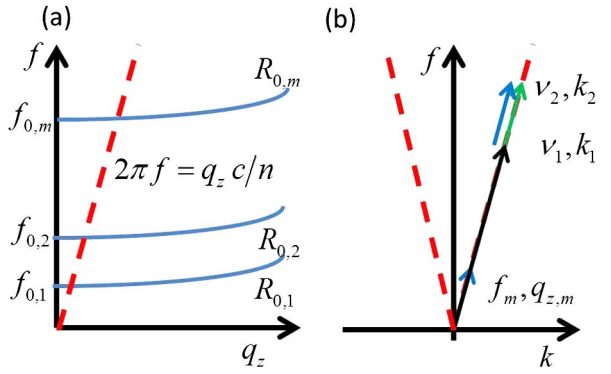

Fig. 1. (a) Solid blue lines: illustration of the dispersion relation between the axial wavenumbers q_z and frequencies f of radial acoustic modes in standard optical fibers. Modal cut-off frequencies are denoted by $f_{0,m}$. Dashed red line: schematic illustration of the dispersion relation of the optical mode of the fiber. The refractive index of the optical mode is noted by n. Intersection points represent frequencies $f_m \approx f_{0,m}$ of acoustic radial modes that can couple between two co-propagating optical waves of frequencies ν_1 and $\nu_2 = \nu_1 + f_m$ and corresponding wavenumbers k_1 and $k_2 = k_1 + q_{z,m}$ [see panel (b)].

For each m, there exists a frequency $f_m \approx f_{0,m}$, for which the phase velocity in the axial direction of $R_{0,m}$ matches that of the optical mode in the fiber: $2\pi f_m/q_{z,m} = c/n$, where n is the effective refractive index of the optical mode (see Fig. 1). Coupling can be introduced between an acoustic mode $R_{0,m}$ and a pair of co-propagating optical waves that are spectrally detuned by f_m through the mechanisms of electro-striction and photo-elasticity. The process is illustrated in Fig. 1(b). The magnitude of density fluctuations in each radial mode scales with the transverse overlap integral between $\Delta\rho_{0,m}(r)$ and $\nabla_T^2 E^2(r)$, where $E(r)$ denotes the transverse profile of the optical field [25,26]. While the axial wavenumber components of the acoustic waves taking part in such interactions are nonzero, they are nevertheless much smaller than the corresponding transverse components: $q_{z,m} \ll 2\pi f_m/V_d$.

Acousto-optic interactions involving radial modes are often referred to as forward stimulated Brillouin scattering [26], guided acoustic wave Brillouin scattering [21], or Raman-like scattering by acoustic phonons [25]. These interactions have been studied extensively since 1985 [21–27]. Experiments show resonant stimulations at frequencies that match very well with the predicted values of $f_{0,m}$ [21–27]. The modes were mapped in standard single-mode fibers [21], highly nonlinear small-core fibers [26], and PCFs [25]. Scattering by radial acoustic modes was found to limit the propagation length of solitons [34] and distort modulated signals [27]. The temperature dependence of $f_{0,m}$ was characterized in standard fibers [35] and in PCFs [36,37]. The thermal coefficient of the resonance frequencies in standard fibers is $(\partial f_{0,m}/\partial T)/f_{0,m} = 93$ ppm/K [35], where T denotes temperature, the same as that of backward stimulated Brillouin scattering. The strain dependence of the radial modes frequencies was investigated as well [38].

3. Probing the Acoustic Modes with an Optical Signal Wave

In our experiments, radial acoustic modes are driven by the spectral components of intense, isolated, and short pump pulses at a central optical wavelength λ_p. The acoustic vibrations induce refractive index perturbations Δn, which follow the propagation of the pump pulses. The magnitude of Δn is very weak [21,26]. Nevertheless, they may introduce changes in the phase delay of a co-propagating signal wave at a different wavelength λ_s [21]. The signal acquires an additional phase delay of $\Delta\varphi = (2\pi/\lambda_s) \cdot \Delta n \cdot L$, where L is the entire length of the fiber. A counter-propagating signal wave, on the other hand, is subject to negligible phase delay variations. The additional phase delay of the signal is therefore nonreciprocal. The relatively weak signal does not affect the acoustic waves. The phase delays are measurable in standard fibers when L is on the order of tens of meters or longer. Kang *et al.* used a Sagnac interferometer loop configuration to convert nonreciprocal phase variations into changes in the intensity of the output signal [25]. We adapt this approach in our sensor platform (see Section 3).

B. Impedance of Surrounding Media and the Acoustic Lifetime

The optical pump wave stimulates an acoustic impulse in the core of the fiber, which represents a superposition of multiple radial modes. The acoustic impulse spreads and radiates outward from the core and reaches the outer boundary of the cladding after $0.5t_r \equiv a/V_d$ seconds (see Fig. 2). Part of the acoustic wave

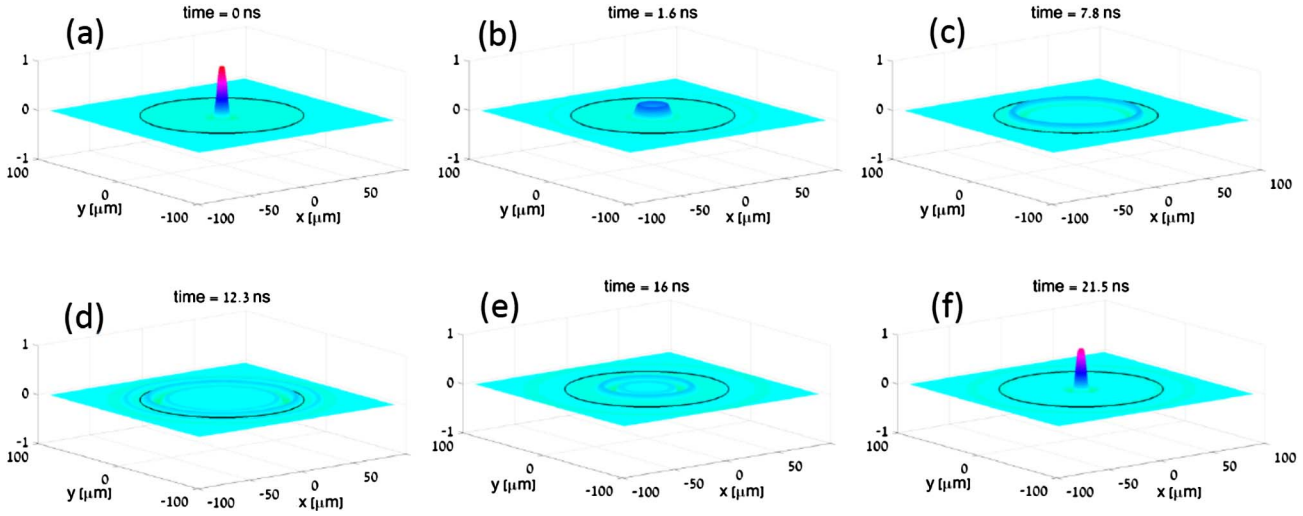

Fig. 2. Illustrations of the acoustic density variations profile $\Delta\rho$ as a function of transverse coordinates x, y, following stimulation by a short pump pulse that is confined to the core of a standard fiber. The black lines mark the outer boundary of the fiber cladding. The density fluctuations are linear combinations of the transverse profiles $\Delta\rho_{0,m}(x,y)$ of individual radial modes $R_{0,m}$ oscillating at respective frequencies $f_{0,m}$. Panels (a)–(f) present $\Delta\rho$ at different instances, noted above each panel. Acoustic impulses form across the core of the fiber at intervals of $t_r \approx 20.83$ ns.

magnitude is reflected back toward the core, while another part is transmitted to the surrounding medium.

An echo of the acoustic impulse reforms within the core of the fiber once every $t_r \approx 20.83$ ns. Each impulse echo is weaker than the previous one, due to transmission losses at the cladding boundary as well as internal dissipation within the silica fiber. Therefore, the acoustic field within the core consists of an infinite series of decaying impulses, separated by t_r.

The reflectivity coefficient of the acoustic field magnitude is determined by the acoustic impedance of silica fiber Z_f and that of the outside medium Z_o [39]:

$$|r_{\mathrm{mir}}| = |Z_f - Z_o|/(Z_f + Z_o). \tag{3}$$

The acoustic impedance equals the product of the material density and its acoustic velocity [39]. The impedance values for silica, deionized water, and ethanol at room temperature are 13.19e6, 1.496e6, and 0.953e6 kg/(m^2 · s), respectively [40]. The acoustic impedance of air is much smaller: 416 kg/(m^2 · s) [40]. It is assumed hereunder that the impedances are independent of the acoustic frequency.

The oscillations lifetime τ_m of an individual mode $R_{0,m}$ is given by

$$\frac{1}{\tau_m} = \frac{1}{\tau_{\mathrm{int},m}} + \frac{1}{\tau_{\mathrm{mir}}} = \frac{1}{\tau_{\mathrm{int},m}} + \frac{1}{t_r}\ln\left(\frac{1}{|r_{\mathrm{mir}}|}\right). \tag{4}$$

In Eq. (4), τ_{mir} is the lifetime due to transmission losses at the boundary, and $\tau_{m,\mathrm{int}}$ denotes the acoustic lifetime associated with internal dissipation, diameter inhomogeneity, and ellipticity of the fiber, and all other sources of loss.

Our proposed sensing protocol is the following: with prior knowledge of $\tau_{m,\mathrm{int}}$, measurements of the decay time constant of stimulated $R_{0,m}$ modes may recover the acoustic reflectivity coefficient at the cladding boundary and hence the acoustic impedance of the surrounding medium. The measurements do not rely on the refractive index or absorption spectrum of the medium under test. Furthermore, since both the stimulation and probing of the acoustic modes are carried out from within the core, no direct spatial overlap is necessary between optical waves and the analyzed medium.

3. EXPERIMENTAL RESULTS

A. Experimental Setup

A schematic illustration of the experimental setup is provided in Fig. 3 [25,41]. Light from a laser diode source ($\lambda_p =$ 1560 nm) was amplitude modulated in a semiconductor optical amplifier (SOA), driven by repeating current pulses of 20 ns duration and 20 μs period. The SOA was necessary to achieve an extinction ratio that was higher than 30 dB. However, the available device could not support shorter pulses. To that end, the pump pulses were further modulated to 1 ns duration with the same period by an electro-optic Mach–Zehnder amplitude modulator. The waveform generators driving the SOA and amplitude modulator were properly synchronized. The pump wave was amplified by an erbium-doped fiber amplifier (EDFA) and launched into a section of standard, single-mode fiber under test (FUT). Due to the low duty cycle and high extinction ratio of the modulation, high peak power levels of pump pulses could be obtained at the EDFA output. The peak power level was adjusted to 4.3 W.

The FUT was placed within a Sagnac loop ([25,41] (see Fig. 3). A signal wave from a second laser diode at $\lambda_s = 1550$ nm was launched into the loop in both directions. The phase delay of the clockwise-propagating signal wave was modified by radial acoustic modes stimulated by the pump pulses, whereas the counterclockwise-propagating signal waves were subject to much smaller phase perturbations, as discussed above. A polarization controller was used to adjust the bias value of the nonreciprocal phase delay within the loop. For sufficiently small nonreciprocal phase delay variations $\Delta\varphi \ll \pi$, changes in the signal power at the loop output were linearly proportional to $\Delta\varphi$.

An optical bandpass filter (BPF) was connected to the FUT within the loop at the output end of the pump wave. The BPF allowed the signal wave to propagate in both directions, whereas

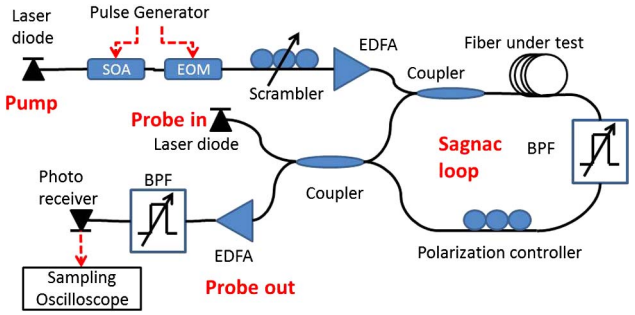

Fig. 3. Schematic illustration of the experimental setup used in the stimulation and probing of radial guided acoustic modes in standard fibers. SOA, semiconductor optical amplifier; EDFA, erbium-doped fiber amplifier; BPF, bandpass filter; EOM, electro-optic modulator.

the pump pulses were blocked from reaching the loop output. The output signal wave was detected by a broadband photodetector and sampled by a real-time digitizing oscilloscope at a 1 GHz bandwidth. The sampled traces were averaged over 8192 repeating pump pulses and analyzed using offline signal processing.

The pump pulses may also stimulate torsional-radial acoustic modes in the fiber, denoted as $TR_{2,m}$ [42]. The resonant spectra of these modes overlap those of $R_{0,m}$ modes, and their excitation interferes with the data analysis. The $TR_{2,m}$ modes introduce birefringence and polarization-dependent scattering of the signal wave [42]. In order to suppress the contribution of these modes, a polarization scrambler was placed along the input path of the pump wave. The effect of the $TR_{2,m}$ modes on the output signal wave was canceled out of the averaged output traces.

B. Results: Stripped Fiber in Deionized Water, Ethanol, and Air

In a first set of experiments, a 30-m-long section of FUT was stripped of its polymer coating using sulfuric acid. Figure 4(a) shows an example of the signal output trace $V(t)$ as a function of time t, with the FUT exposed in the air. A magnified view of the first 200 ns of the output trace is shown in Fig. 4(b). The first 10 ns of the trace were disregarded due to the residual leakage of the intense pump pulses and cross-phase modulation effects (not shown). A series of impulses separated by t_r is observed, as expected.

The power spectral density $|V(f)|^2$ of the output trace is presented in Fig. 4(c). Multiple resonances corresponding to the $R_{0,m}$ modes are observed. Table 1 lists the experimentally obtained frequencies $f_{0,m}$ alongside the predicted values {Eq. (1), [21,26]}. Excellent agreement is achieved. The calculated frequencies are consistently higher by $0.7 \pm 0.15\%$. This difference possibly suggests a cladding diameter of 125.8 μm, which is within the specified tolerances. Figure 4(d) presents the measured relative power in each mode $|V(f_{0,m})|^2$ alongside the expected modal strengths, calculated based on the transverse profiles of the acoustic modes and the optical mode and the power spectral density of the pump pulses (see Supplement 1 for a detailed analysis). The experimental uncertainty among consecutive measurements of modal strengths is bound by ±5%. Good quantitative agreement is found between the model and the measurements (Table 1). The stimulation of the lowest-order modes $m = 1, 2$ is inefficient due to the small overlap between their broad transverse profiles

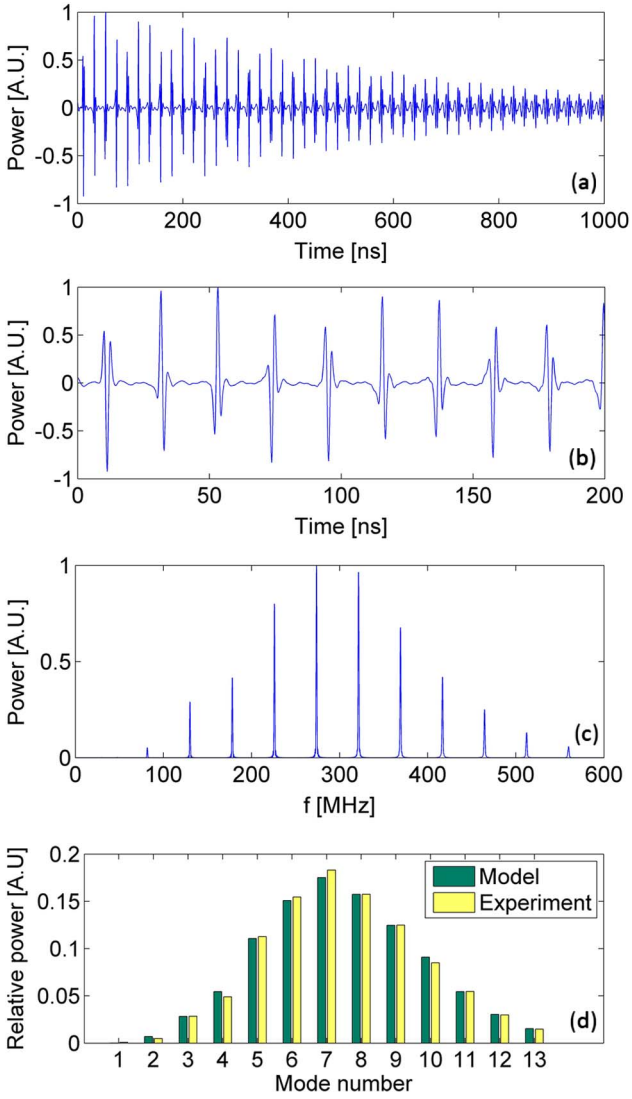

Fig. 4. (a) Measured power of the signal wave as a function of time at the output of the Sagnac interferometer loop. The fiber under test was stripped of its polymer coating and kept exposed in the air. (b) Magnified view of panel (a) in its first 200 ns. A decaying sequence of impulses, separated by $t_r \sim 20.83$ ns, is observed. (c) Power spectral density of the measured output signal trace. The spectrum consists of a series of discrete modes whose frequencies match the cut-off frequencies of the radial acoustic modes (see Table 1). (d) Measurement and calculation of the peak power spectral density in each mode.

and that of the electro-strictive driving force. The stimulation of modes $m \geq 13$ is limited by the bandwidths of the pump pulses.

Figure 5(a) shows $V(t)$ with the FUT immersed in deionized water and in a mixture of 95% ethanol and 5% methanol. Compared with measurements of the FUT in air, the series of impulses in these traces decays much more quickly. The traces were digitally filtered to select contributions of individual modes, $m = 3$ to 11. Figure 5(b) shows the filtered traces for mode $m = 5$. The modal oscillations are well characterized by an exponential decay, with a single time constant for each mode. The decay is dominated by acoustic transmission losses at the outer boundary of the fiber cladding. The lifetimes of individual modes τ_m, with the FUT in deionized water and ethanol, are shown in the lower two curves of Fig. 5(c).

Table 1. Measured and Calculated Frequencies and Relative Peak Power Spectral Densities of Guided Radial Acoustic Modes in a Standard Fiber

Mode	Measured Freq. (MHz)	Calculated Freq. (MHz)	Measured Rel. Power	Calculated Rel. Power
1	30.34	30.53	0.00084	0.00016
2	81.66	82.07	0.0048	0.007
3	130.1	130.8	0.0282	0.0282
4	178.1	179.0	0.049	0.0546
5	226.0	227.2	0.1127	0.1106
6	273.3	275.3	0.1545	0.1509
7	321.4	323.3	0.183	0.1752
8	369.1	371.4	0.1575	0.1574
9	416	419.4	0.1247	0.1247
10	464	467.3	0.0849	0.091
11	511	515.4	0.0547	0.0544
12	559	563.3	0.0299	0.0305
13	607	611.3	0.0149	0.0154

The assessment of acoustic reflectivity $|r_{\mathrm{mir}}|$ at the cladding boundary requires knowledge of the intrinsic losses of the acoustic modes [Eq. (4)]:

$$|r_{\mathrm{mir}}| = \exp\left(-\frac{\tau_{\mathrm{int},m} - \tau_m}{\tau_{\mathrm{int},m} \cdot \tau_m} t_r\right). \quad (5)$$

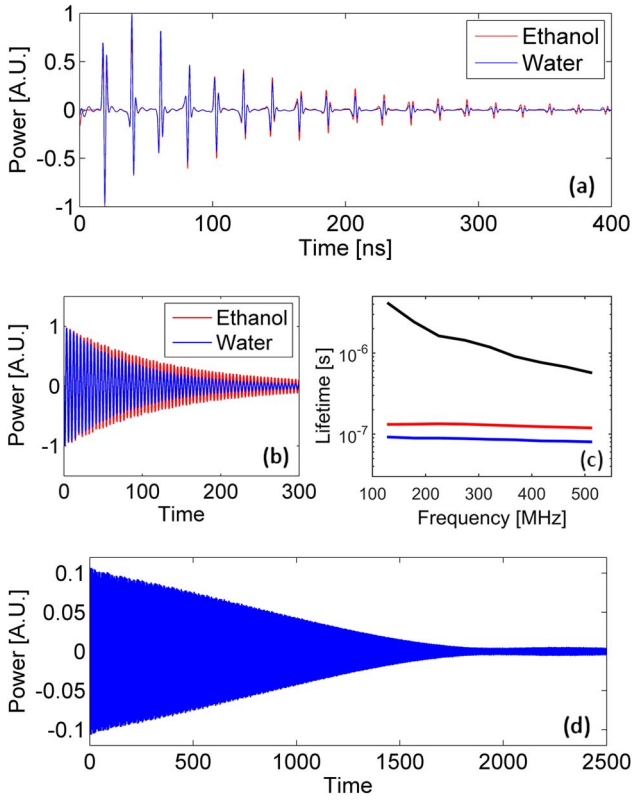

Fig. 5. (a) Measured power of the signal wave with the fiber under test immersed in deionized water (blue) and ethanol (red). (b) Measured oscillations of acoustic mode $R_{0,5}$ at 226 MHz, obtained by digital filtering of the traces of panel (a). Time scale in ns. (c) Experimentally obtained lifetimes of radial acoustic modes $m = 3$ through 11, with the fiber under test in air (black line), water (blue line), and ethanol (red line). (d) Measured oscillations of acoustic mode $R_{0,5}$ at 226 MHz with the fiber under test in air, obtained by digital filtering of the trace of Fig. 4(a). Time scale in ns.

The intrinsic lifetimes $\tau_{\mathrm{int},m}$ were estimated based on measurements taken of the FUT in air. The oscillations of the individual modes were filtered as described above. An example for $R_{0,5}$ is shown in Fig. 5(d). Due to the low acoustic impedance of air, reflectivity at the cladding boundary practically equals unity for all modes. The acoustic resonances with the FUT in air are broadened by inhomogeneity in radius a along the fiber length [26], and hence their temporal decay cannot be described by a single time constant. The effective intrinsic lifetimes $\tau_{m,\mathrm{int}}$ were therefore estimated based on the first 150 ns of the filtered traces, a duration that is comparable with modal lifetimes observed with the FUT immersed in test liquids. The estimated lifetimes do not fully describe the entire dynamics of modal oscillations with the fiber in air. Nevertheless, they account for the acoustic losses mechanisms, other than transmission at the boundaries, within the time frame that is relevant to the analysis of liquids. The estimates of $\tau_{m,\mathrm{int}}$ are shown in the upper trace of Fig. 5(c).

Figure 6(a) presents the experimentally obtained acoustic impedances of deionized water and ethanol based on the time constants of modes $m = 3$ to 11. The results were averaged over 30 consecutive experiments. The acoustic impedances are independent of the frequency, supporting previous assumptions. The experimental impedances are 1.475e6 ± 0.01e6 km/(m^2 · s) for deionized water and 0.95e6 ± 0.03e6 km/(m^2 · s) for ethanol. The corresponding values reported in the literature are 1.485e6 and 0.953e6 km/(m^2 · s), respectively [32]. The experimental uncertainties represent the differences between impedance estimates based on different modes. Impedance variations among repeating analyses of a given medium using an individual mode are below 0.1%. The measurements and reference data agree to within less than 1%. The results demonstrate that the fiber-sensor setup can quantitatively measure the acoustic impedance of surrounding liquids outside the cladding.

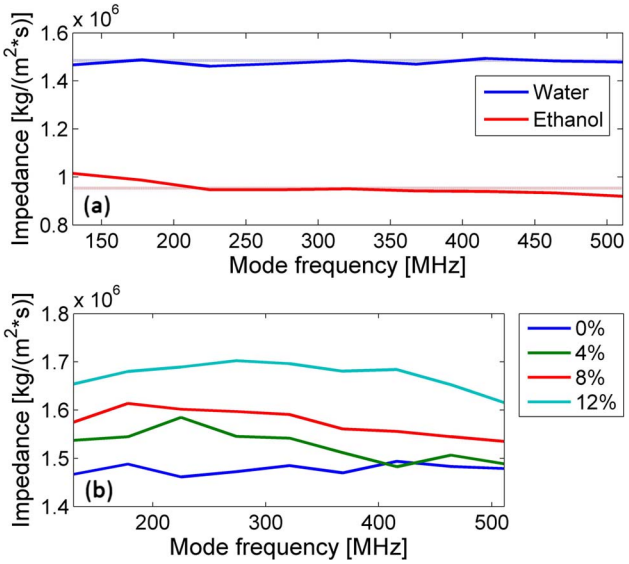

Fig. 6. (a) Solid lines: measured acoustic impedances of deionized water (blue) and ethanol (red) as a function of the frequency of acoustic radial modes. Dashed lines: corresponding reference acoustic impedance values [36]. (b) Measured acoustic impedances of solutions of deionized water as a function of the frequency of acoustic radial modes. Colors denote aqueous solutions with dissolved NaCl at relative weight ratios of 0, 4%, 8%, and 12% (see legend).

Table 2. Measured Acoustic Impedance of Liquids Under Test and Corresponding Reference Values [in Units of 1e6 kg/(m² · s)]

Liquid	Measured Impedance	Reference Impedance
Ethanol	0.95 ± 0.03	0.953 [32]
Deionized water	1.475 ± 0.01	1.485 [32]
Water + 4% NaCl	1.52 ± 0.03	1.571 [33]
Water + 8% NaCl	1.57 ± 0.03	1.664 [33]
Water + 12% NaCl	1.67 ± 0.03	1.763 [33]

C. Results: Fiber in Solutions of Dissolved Salt in Deionized Water

The acoustic impedance of aqueous solutions is known to change with the concentration of dissolved salts [33]. In a second set of experiments, the FUT was immersed in several solutions of deionized water with 4%, 8%, and 12% relative weight of NaCl. The acoustic impedances of the solutions were recovered using the experimental procedure described in the previous subsection. The results are plotted in Fig. 6(b). The measured impedances of deionized water are shown again for comparison. The results are summarized in Table 2.

The measurements clearly distinguish between the four solutions. The acoustic impedance is seen to increase with the level of salinity, in agreement with the expectations. Quantitative agreement between the results and the previously stated values is partial: we observed 1.2% increase in impedance per 1% increase in the relative weight of dissolved salt, as opposed to a corresponding impedance change by 1.6% reported in the literature (Ref. [33], see Table 2). The reasons for this disagreement are still under study. Despite these differences, the results illustrate the ability of the sensor setup to resolve fine changes in acoustic impedance.

4. CONCLUSIONS

In this work, we proposed and demonstrated an optomechanical fiber sensor that is able to measure the acoustic impedances of liquid media outside the cladding of standard single-mode fibers. The outer boundary of the cladding is probed by guided radial acoustic modes of the fiber structure. Both the stimulation and the monitoring of acoustic modes are carried out by optical waves that are confined to the core. Unlike previous sensors of liquids, no structural modification of the standard fiber was necessary. The results represent a new paradigm toward one of the basic challenges of fiber-optic sensor research.

The impedances of deionized water and ethanol were measured and are in excellent agreement with literature values. The analysis also identified fine changes between the impedances of aqueous solutions with different concentrations of dissolved salt. The accuracy of the proposed sensor platform is already relevant to the remote monitoring of industrial processes involving heavy ionic solutions, such as in electro-chemistry or desalination of water. However, the method may be further generalized for the monitoring and detection of various analytes outside the fiber if the cladding is treated with a proper antibody.

Measurements of refractive indexes are prone to ambiguity and uncertainty due to the thermo-optic effect. The optomechanical sensor demonstrated in this work can be immune to this issue. Temperature changes may be identified and calibrated based on tracking the exact resonance frequencies of the acoustic modes or through standard Brillouin analysis.

Stronger pump pulses would support the use of shorter FUTs, toward the meter scale. It should be noted, however, that the pump path within the Sagnac loop inevitably contains residual segments of coated fibers connecting with components such as couplers or BPFs. The acoustic characteristics of these sections should be taken into account in the analysis of data collected over very short FUTs. In the current experiment, comparatively short pump pulses were used in order to excite multiple modes. Alternatively, it is possible to maximize the excitation of an individual mode, for example, by matching the pump pulse duration with half its period. Sine-wave modulation of the pump wave at the acoustic resonance frequency may be employed as well [41].

Finally, the measurements currently rely on the interaction between the co-propagating pump and signal waves and do not support distributed analysis. Future research would concentrate on trying to remove this limitation.

Funding. Bar-Ilan University.

See Supplement 1 for supporting content.

REFERENCES

1. B. Culshaw and J. Dakin, *Optical Fiber Sensors: Principles and Components* (Artech House, 1988).
2. E. Udd and W. B. Spillman, eds., *Fiber Optic Sensors: An Introduction for Engineers and Scientists*, 2nd ed. (Wiley, 2011).
3. B. Lee, "Review of the present status of optical fiber sensors," Opt. Fiber Technol. **9**, 57–79 (2003).
4. K. T. V. Grattan and B. T. Meggit, eds., *Optical Fiber Sensor Technology*, Vol. **4** of Chemical and Environmental Sensing (Kluwer Academic, 2010).
5. T. Ritari, J. Tuominen, H. Ludvigsen, J. Petersen, T. Sørensen, T. Hansen, and H. Simonsen, "Gas sensing using air-guiding photonic bandgap fibers," Opt. Express **12**, 4080–4087 (2004).
6. T. G. Euser, J. S. Y. Chen, M. Scharrer, P. St.J. Russell, N. J. Farrer, and P. J. Sadler, "Quantitative broadband chemical sensing in air-suspended solid-core fibers," J. Appl. Phys. **103**, 103108 (2008).
7. D. K. C. Wu, B. T. Kuhlmey, and B. J. Eggleton, "Ultrasensitive photonic crystal fiber refractive index sensor," Opt. Lett. **34**, 322–324 (2009).
8. I. Dicaire, A. De Rossi, S. Combrié, and L. Thévenaz, "Probing molecular absorption under slow-light propagation using a photonic crystal waveguide," Opt. Lett. **37**, 4934–4936 (2012).
9. S. W. James and R. P. Tatam, "Optical fibre long-period grating sensors: characteristics and application," Meas. Sci. Technol. **14**, R49–R61 (2003).
10. J.-K. Yoon, G. W. Seo, K. M. Cho, E. S. Kim, S. H. Kim, and S. W. Kang, "Controllable in-line UV sensor using a side-polished fiber coupler with photofunctional polymer," IEEE Photon. Technol. Lett. **15**, 837–839 (2003).
11. W. Liang, Y. Huang, Y. Xu, R. K. Lee, and A. Yariv, "Highly sensitive fiber Bragg grating refractive index sensors," Appl. Phys. Lett. **86**, 151122 (2005).
12. P. Lu, L. Men, K. Sooley, and Q. Chen, "Tapered fiber Mach-Zehnder interferometer for simultaneous measurement of refractive index and temperature," Appl. Phys. Lett. **94**, 131110 (2009).
13. C. L. Tien, H. W. Chen, W. F. Liu, S. S. Jyu, S. W. Lin, and Y. S. Lin, "Hydrogen sensor based on side-polished fiber Bragg gratings coated with thin palladium film," Thin Solid Films **516**, 5360–5363 (2008).
14. E. Preter, B. Preloznik, V. Artel, C. N. Sukenik, D. Donlagic, and A. Zadok, "Monitoring the evaporation of fluids from fiber-optic micro-cell cavities," Sensors **13**, 15261–15273 (2013).
15. Z. L. Ran, Y. J. Rao, W. J. Liu, X. Liao, and K. S. Chiang, "Laser-micromachined Fabry–Perot optical fiber tip sensor for high-resolution temperature-independent measurement of refractive index," Opt. Express **16**, 2252–2263 (2008).

16. E. Preter, R. A. Katims, V. Artel, C. N. Sukenik, D. Donlagic, and A. Zadok, "Monitoring and analysis of pendant droplets evaporation using bare and monolayer-coated optical fiber facets," Opt. Mater. Express **4**, 903–915 (2014).
17. M. Choi, M. Humar, S. Kim, and S. H. Yun, "Step-index optical fiber made of biocompatible hydrogels," Adv. Mater. **27**, 4081–4086 (2015).
18. S. Nizamoglu, M. C. Gathe, M. Humar, M. Choi, S. Kim, K. S. Kim, S. K. Hahn, G. Scarcelli, M. Randolph, R. W. Redmond, and S. H. Yun, "Bioabsorbable polymer optical waveguides for deep-tissue photomedicine," Nat. Commun. **7**, 10374 (2016).
19. F. G. Omenetto and D. L. Kaplan, "A new route for silk," Nat. Photonics **2**, 641–643 (2008).
20. K. Hey Tow, D. Chow, F. Vollrath, I. Dicaire, T. Gheysens, and L. Thévenaz, "Spider silk: a novel optical fibre for biochemical sensing," Proc. SPIE **9634**, 96347D (2015).
21. R. M. Shelby, M. D. Levenson, and P. W. Bayer, "Guided acoustic-wave Brillouin scattering," Phys. Rev. B **31**, 5244–5252 (1985).
22. A. S. Biryukov, M. E. Sukharev, and E. M. Dianov, "Excitation of sound waves upon propagation of laser pulses in optical fibers," Quantum Electron. **32**, 765–775 (2002).
23. P. St.J. Russell, D. Culverhouse, and F. Farahi, "Experimental observation of forward stimulated Brillouin scattering in dual-mode single-core fibre," Electron. Lett. **26**, 1195–1196 (1990).
24. P. St.J. Russell, D. Culverhouse, and F. Farahi, "Theory of forward stimulated Brillouin scattering in dual-mode single-core fibers," IEEE J. Quantum Electron. **27**, 836–842 (1991).
25. M. S. Kang, A. Nazarkin, A. Brenn, and P. St.J. Russell, "Tightly trapped acoustic phonons in photonic crystal fibers as highly nonlinear artificial Raman oscillators," Nat. Phys. **5**, 276–280 (2009).
26. J. Wang, Y. Zhu, R. Zhang, and D. J. Gauthier, "FSBS resonances observed in standard highly nonlinear fiber," Opt. Express **19**, 5339–5349 (2011).
27. E. Peral and A. Yariv, "Degradation of modulation and noise characteristics of semiconductor lasers after propagation in optical fiber due to a phase shift induced by stimulated Brillouin scattering," IEEE J. Quantum Electron. **35**, 1185–1195 (1999).
28. I. S. Grudinin, A. B. Matsko, and L. Maleki, "Brillouin lasing with a CaF_2 whispering gallery mode resonator," Phys. Rev. Lett. **102**, 043902 (2009).
29. M. Tomes and T. Carmon, "Photonic micro-electromechanical systems vibrating at X-band (11-GHz) rates," Phys. Rev. Lett. **102**, 113601 (2009).
30. G. Bahl, K. H. Kim, W. Lee, J. Liu, X. Fan, and T. Carmon, "Brillouin cavity optomechanics with microfluidic devices," Nat. Commun. **4**, 1994 (2013).
31. K. H. Kim, G. Bahl, W. Lee, J. Liu, M. Tomes, X. Fan, and T. Carmon, "Cavity optomechanics on a microfluidic resonator with water and viscous liquids," Light Sci. Appl. **2**, e110 (2013).
32. M. I. Aralaguppi, C. V. Jadar, and T. M. Aminabhavi, "Density, viscosity, refractive index, and speed of sound in binary mixtures of acrylonitrile with methanol, ethanol, propan-1-ol, butan-1-ol, pentan-1-ol, hexan-1-ol, heptan-1-ol, and butan-2-ol," J. Chem. Eng. Data **44**, 216–221 (1999).
33. A. Puttmer, P. Hauptmann, and B. Henning, "Ultrasonic density sensor for liquids," IEEE Trans. Ultrason. Ferroelectr. Freq. Control **47**, 85–92 (2000).
34. L. F. Mollenauer, P. V. Mamyshev, and M. J. Neubelts, "Measurements of timing jitter in filter-guided soliton transmission at 10 Gbit/s and achievement of a 375 Gbit/s-Mm, error-free, at 12.5 and 15 Gbit/s," Opt. Lett. **19**, 704–706 (1994).
35. Y. Tanaka and K. Ogusu, "Temperature coefficient of sideband frequencies produced by depolarized guided acoustic-wave Brillouin scattering," IEEE Photon. Technol. Lett. **10**, 1769–1771 (1998).
36. T. Matsui, K. Nakajima, T. Sakamoto, K. Shiraki, and I. Sankawa, "Structural dependence of guided acoustic-wave Brillouin scattering spectral in hole-assisted fiber and its temperature dependence," Appl. Opt. **46**, 6912–6917 (2007).
37. E. Carry, J.-C. Beugnot, B. Stiller, M. W. Lee, H. Maillotte, and T. Sylvestre, "Temperature coefficient of the high-frequency guided acoustic mode in a photonic crystal fiber," Appl. Opt. **50**, 6543–6547 (2011).
38. Y. Tanaka and K. Ogusu, "Tensile-strain coefficient of resonance frequency of depolarized guided acoustic-wave Brillouin scattering," IEEE Photon. Technol. Lett. **11**, 865–867 (1999).
39. B. Auld, *Acoustic Fields and Waves in Solids* (Krieger, 1990), Vol. **2**.
40. D. R. Lide, ed., *CRC Handbook of Chemistry and Physics* (CRC Press, 2005).
41. Y. Antman, Y. London, and A. Zadok, "Scanning-free characterization of temperature dependence of forward stimulated Brillouin scattering resonances," Proc. SPIE **9634**, 96345C (2015).
42. A. J. Poustie, "Bandwidth and mode intensities of guided acoustic-wave Brillouin scattering in optical fibers," J. Opt. Soc. Am. B **10**, 691–696 (1993).